Biaxial strain-induced enhancement in the thermoelectric performance of monolayer WSe_2*

Wanhuizi Shen(沈婉慧子)[1], Daifeng Zou(邹代峰)[1,2,†], Guozheng Nie(聂国政)[1], and Ying Xu(许英)[1]

[1] School of Physics and Electronic Science, Hunan University of Science and Technology, Xiangtan 411201, China
[2] Shenzhen Key Laboratory of Nanobiomechanics, Shenzhen Institutes of Advanced Technology, Chinese Academy of Sciences, Shenzhen 518055, China

(Received 3 July 2017; revised manuscript received 10 August 2017; published online 30 September 2017)

The effects of biaxial strain on the electronic structure and thermoelectric properties of monolayer WSe_2 have been investigated by using first-principles calculations and the semi-classical Boltzmann transport theory. The electronic band gap decreases under strain, and the band structure near the Fermi level of monolayer WSe_2 is modified by the applied biaxial strain. Furthermore, the doping dependence of the thermoelectric properties of n- and p-doped monolayer WSe_2 under biaxial strain is estimated. The obtained results show that the power factor of n-doped monolayer WSe_2 can be increased by compressive strain while that of p-doping can be increased with tensile strain. Strain engineering thus provides a direct method to control the electronic and thermoelectric properties in these two-dimensional transition metal dichalcogenides materials.

Keywords: monolayer WSe_2, biaxial strain, thermoelectric properties, first-principles

PACS: 72.20.Pa, 72.80.Ga, 31.15.A– **DOI:** 10.1088/1674-1056/26/11/117202

1. Introduction

Thermoelectric materials, which can directly and reversibly convert heat into electricity, have potential applications in power generation and refrigeration. The conversion efficiency of thermoelectric materials is described by the figure of merit, ZT, which is defined as $ZT = S^2\sigma T/\kappa$, where S, σ, and κ are the Seebeck coefficient, electrical conductivity, and thermal conductivity, respectively. A good thermoelectric material must possess a high ZT value. The current researches are focused on enhancing the ZT value by increasing the Seebeck coefficient and electrical conductivity values with reducing the value of thermal conductivity. However, the correlation and coupling among these physical parameters make it extremely difficult to control independently.

The transition-metal dichalcogenides with the formula MX_2 (where M = Mo, W; X = S, Se, Te) have found applications in energy storage, sensing, catalysis, and electronic devices for many years.[1–6] These compounds exhibit a "sandwich" type of structure (X–M–X) in which metal atoms (M) are located in between two layers of chalcogen atoms (X).[7] Some crystals of this group, such as MoS_2 and WSe_2, have been suggested as promising candidates for thermoelectric applications due to the large Seebeck coefficient and low thermal conductivity.[8–14] It was reported that the low-dimensional thermoelectric materials could exhibit much higher ZT values on account of the improved power factor ($S^2\sigma$) caused by quantum confinement effects.[15,16] Recently, two-dimensional (2D) semiconductor materials formed by transition-metal dichalcogenide layered structures have attracted a great deal of interest due to the fact that they possess enhanced thermoelectric performance compared to the corresponding bulks.[8–14] Compared with other 2D transition metal dichalcogenides, the monolayer WSe_2 is found to have an ultralow thermal conductivity, which is one order of magnitude lower than that of MoS_2, suggesting that the monolayer WSe_2 has great application potential in thermoelectric applications.[17] In previous reports, strain engineering was proved as an effective method to tune the electronic structure and thermoelectric properties of semiconductors.[18–20] Recent studies have shown that the thermoelectric properties of Bi_2Te_3 and Sb_2Te_3 can be further improved by the application of strain.[18] It is found that biaxial strain can fine-tune the electronic structure near the Fermi level, and thus it can enhance the transport properties of thermoelectric compounds such as $Cu_2ZnSnSe_4$ and $SrTiO_3$.[19,20] Pardo *et al.* reported that strain can optimize the thermoelectric properties of hole-doped $La_2NiO_{4+\delta}$ using first-principles calculations as well.[21] It was reported that strain engineering can tune the electronic properties of 2D MX_2 (M = Mo, W; X = S, Se, Te),[7–10,22–24] and the strain can be induced easily by growing the transition metal dichalcogenides on flexible substrates. Recently, mechanical strain induced enhancement in the thermoelectric properties have been reported in monolayer ZrS_2 and $PtSe_2$ nanosheets as well.[25,26] However, previous theoretical studies mainly focus on the effect of mechanical strains on the electronic properties of the monolayer of MX_2 (where M = Mo, W; X = S, Se, Te),[7–10] and few studies have investigated the influence of strain engineering on the thermoelectric

*Project supported by the National Natural Science Foundation of China (Grant No. 11627801) and the Research Foundation of Education Bureau of Hunan Province of China (Grant Nos. 15B083 and 17B090).

†Corresponding author. E-mail: daifengzou@gmail.com

© 2017 Chinese Physical Society and IOP Publishing Ltd

properties of WSe_2 monolayer. In order to understand the relationship between their electronic structures and thermoelectric properties under strain, explore the effect of strain on their thermoelectric properties, and further enhance the thermoelectric performance of monolayer WSe_2, it is necessary to investigate the effect of strain on the electronic structures and thermoelectric properties of monolayer WSe_2.

2. Computational methods

First-principles based on the Vienna *ab initio* simulation package (VASP)[27] is used to calculate the structural and electronic properties of monolayer WSe_2. For the structure optimization and the electronic structure calculations, we employ the Perdew–Burke–Ernzerhof (PBE)[28] generalized gradient approximation (GGA) and projector augment wave (PAW)[29] pseudopotentials, and the cutoff energy of the plane-wave expansion is set at 450 eV. For each monolayer, a vacuum region of 15 Å is added perpendicular to the WSe_2 monolayer plane so that the interactions between the periodic images can be neglected. A well-converged Monkhorst–Pack k-point set ($13 \times 13 \times 1$) is used for the Brillouin zone sampling. Spin–orbit coupling (SOC) were considered here because it has very important effects on electronic structures and power factor of transition-metal dichalcogenides.[26,30,31]

The transport calculations of the Seebeck coefficient S and electronic conductivity over relaxation time σ/τ are performed through solving the Boltzmann transport equations within the rigid band approximation (RBA)[32] as implemented in the BoltzTraP package.[33] The constant relaxation time approximation,[34] which assumes τ to be energy-independent, is used to estimate the transport properties, and this approximation has successfully predicted the transport properties for many thermoelectric compounds.[18–21,35–38] To get reasonable transport properties, a more dense k-mesh ($35 \times 35 \times 1$) was used for WSe_2 monolayer in the Monkhorst–Pack scheme, and it can guarantee convergence and obtain accurate carrier group velocities, which is essential for determining the electrical transport properties of WSe_2 monolayer.

3. Results and discussion

3.1. Crystal structure

Bulk WSe_2 is crystallized in the hexagonal structure with the $P63/mmc$ space group. The hexagonal structure of WSe_2 with the lattice parameters $a = b = 3.282$ Å and $c = 12.96$ Å[39] was taken as the starting point for the geometry relaxation. We then built the structure of WSe_2 monolayer, starting with the lattice parameters of the bulk relaxed WSe_2. The WSe_2 monolayer was placed in a large supercell with about 15 Å of vacuum between the periodic replica. The calculated values of a (3.314 Å) are very close to other reported theoretical results.[11] The top and side views of the fully relaxed structural configurations of monolayer WSe_2 are shown in Fig. 1. We then apply a biaxial strain on monolayer WSe_2 by changing the in-plane lattice parameter a, relaxing the structure along the out-of-plane lattice parameter c. The biaxial in-plane strain is defined by $\Delta a/a_0 \times 100\% = (a - a_0)/a_0 \times 100\%$, where a_0 is the unstrained lattice constant, and a is the in-plane lattice constant of the strained state. The calculated lattice parameters of WSe_2 monolayer at different strains are listed in Table 1. As we can see from Table 1, the W–Se bond lengths, Se–Se bond lengths, and Se–W–Se bond angles vary linearly with the applied strain. The result shows that it has a significant impact on the electronic structure of strained monolayer WSe_2, as discussed below.

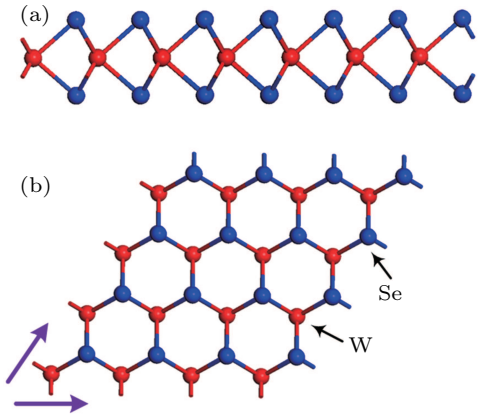


Fig. 1. (color online) Side view (a) and top view (b) of monolayer WSe_2. The figure shows a 4×4 supercell, and the arrows show the application of biaxial strain.

Table 1. Calculated structural parameters for monolayer WSe_2 as a function of the applied strains.

Strain/%	d_{W-Se}/Å	d_{Se-Se}/Å	θ (Se–W–Se)
–6	2.5147	3.5157	88.6967
–5	2.5189	3.4881	87.6389
–4	2.5233	3.4608	86.5906
–3	2.5281	3.4339	85.5531
–2	2.5333	3.4075	84.5262
–1	2.5388	3.3816	83.5129
0	2.5457	3.3591	82.5613
1	2.5511	3.3316	81.5313
2	2.5579	3.3077	80.5661
3	2.5651	3.2846	79.6190
4	2.5728	3.2623	78.6922
5	2.5808	3.2407	77.7828
6	2.5892	3.2199	76.8936

3.2. Electronic structure

Band structures of the monolayer WSe_2 under different biaxial strains are shown in Fig. 2. We can see from Fig. 2(c) that unstrained monolayer WSe_2 shows the direct band gap feature, the conduction band minimum (CBM) and the valence band maximum (VBM) are both located at K. When the tensile strain is applied, the bands at the Γ point approach the Fermi

level gradually, and the VBM of unstrained monolayer WSe_2 near the K point is finally changed to the Γ point under 6% tensile strain, see Figs. 2(d)–2(f), resulting in a transition from a direct to an indirect band gap semiconductor under strain. Meanwhile, the CBM is gradually lowered as the increasing strain, as shown in Figs. 2(d)–2(f). As a result, it can be found that the energy band gap decreases with the increase of applied strain, as summarized in Fig. 3. In the case of compressive strain, the variations in the energy band structures are then more complex: the position of the CBM changes from the K-point to in between the K-point and the Γ-point, while VBM remains at the K-point (see Figs. 2(a) and 2(b)), leading to a change in the nature of the energy gap for the WSe_2 monolayer from direct to indirect. Moreover, the energy gap of the WSe_2 monolayer decreases with the increase of applied strain, as illustrated in Fig. 3. Such strain effect on CBM or VBM can be found in other transition-metal dichalcogenides.[10,31] Since the transport properties of thermoelectric materials are determined by the band gap and the feature of band edge structure near Fermi,[19,30] the change of bandgap and band structure under biaxial strain will have a great influence on the transport properties of WSe_2 monolayer.

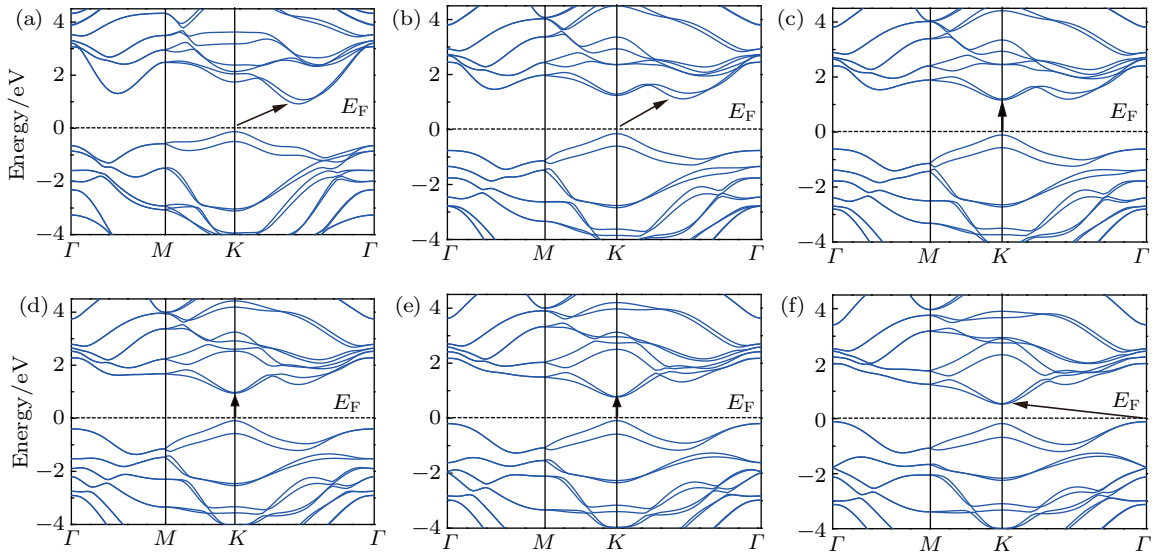


Fig. 2. (color online) Band structures of the monolayer WSe_2 under different biaxial strains: (a) −6%, (b) −1%, (c) 0%, (d) 2%, (e) 4%, (f) 6%. The red arrows point from valence band maximum to conduction band minimum. The Fermi level is set to be 0 eV.

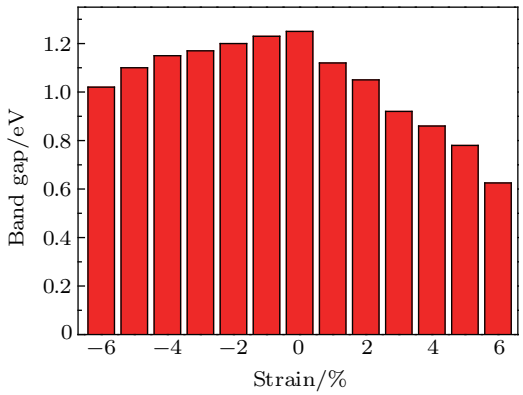


Fig. 3. (color online) Calculated band gaps of monolayer WSe_2 as a function of the applied biaxial strains.

To gain more insight into the changes in the electronic properties of WSe_2 monolayer under strains, the partial densities of states (PDOS) of WSe_2 monolayer under different applied strains are shown in Fig. 4. It can be seen that the CBM of unstrained monolayer WSe_2 primarily comes from hybridization of the W d_{z^2} and the W d_{xy,x^2-y^2} orbitals, whereas the VBM is dominated by the W d_{xy,x^2-y^2} orbital with very small contributions of the W d_{z^2} orbital, and the W $d_{xz,yz}$ orbital does not contribute at all to the band edges. When the tensile strain is applied, as shown in Figs. 4(d)–4(f), the W d_{z^2} orbital of CBM and the W d_{z^2} orbital near VBM shift toward the Fermi level, and it weakens the coupling between the W d_{z^2} and the Se p orbitals. The shift of W d orbital near Fermi level is caused by the increase in W–Se bond length under tensile strain, and it will shrink the band gap and change the shape of the band structure near Fermi level. For compressively strained monolayer WSe_2, the decreasing W–Se bond length strengthens the coupling between the W d_{z^2} and the Se p orbitals, resulting in that the energy positions of these peaks of the W d_{z^2} orbital near VBM shift to lower energy, and the hybridized W d_{z^2} and d_{xy,x^2-y^2} orbitals which constitute CBM move to the Fermi level, as shown in Figs. 4(a) and 4(b). This observation is in good agreement with previous theoretical studies.[7] The shift of W d orbital near Fermi level contributes to a decrease of band gap with the increase in strain. Meanwhile, the change of PDOS of WSe_2 monolayer under biaxial strain reflects the essence of the change of the

sensitive dependence of band edge structure near Fermi on the applied strain. On the other hand, the slope of DOS near the Fermi level can reflect the transport properties of thermoelectric materials.[40,41] Thus, we can deduce that thermoelectric performance of WSe_2 monolayer can be tuned by applying biaxial strain which will be further discussed below.

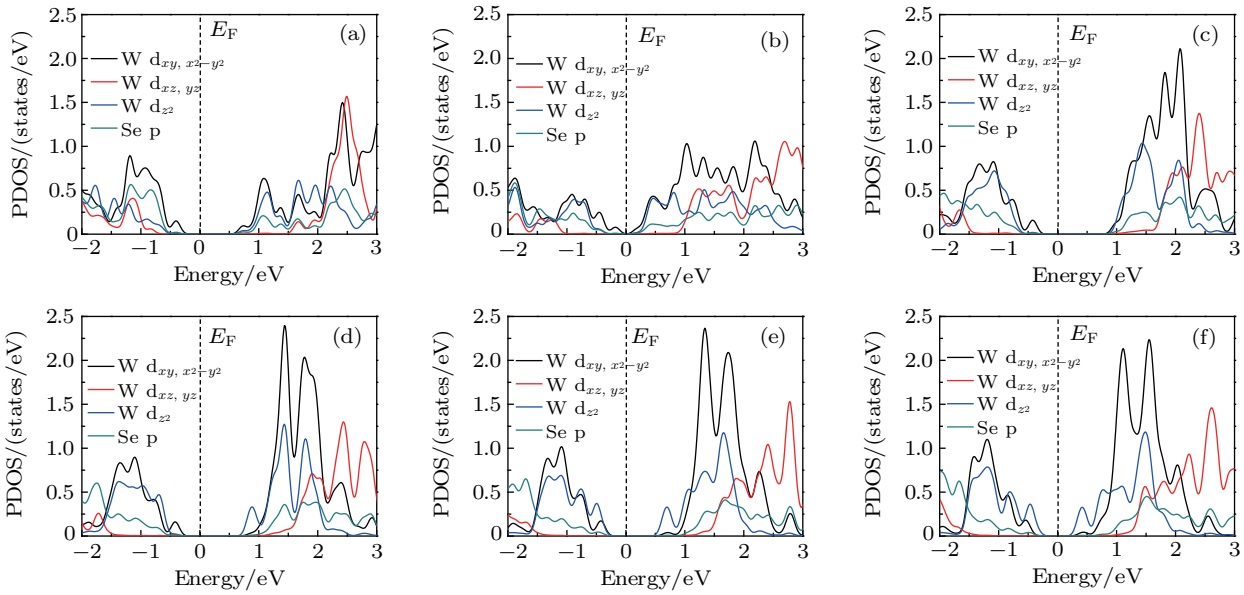


Fig. 4. (color online) Partial densities of states of monolayer WSe_2 under different biaxial strains: (a) −6%, (b) −1%, (c) 0%, (d) 2%, (e) 4%, (f) 6%.

3.3. Thermoelectric properties

Based on the calculated electronic structure, the Seebeck coefficient S and relaxation time scaled electronic conductivity σ/τ can be obtained using the semi-classical Boltzmann theory in conjunction with rigid band and constant relaxation time approximations. The results for the Seebeck coefficient, electrical conductivity, and power factors of n-doped monolayer WSe_2 as a function of the number of electrons per unit cell are shown in Fig. 5. Since the thermoelectric performance peaks occur at 900 K, all the results of the transport properties in monolayer WSe_2 are presented at this temperature. As seen in Fig. 5(a), the Seebeck coefficients at typical values of strain decrease with increased doping levels. In order to make a comparison of thermoelectric properties under strains at the same doping level, the Seebeck coefficients as a function of the biaxial strain are shown in the inset of Fig. 5(a). For these calculations, the n-type doped level is fixed at 7×10^{19} cm^{-3}, which is the optimized value for n-type doped monolayer WSe_2, and it is slightly higher than the theoretically optimized carrier concentration of MoS_2 monolayer.[8] As we can see from the inset of Fig. 5(a), the Seebeck coefficient increases under compressive strain, while it decreases under tensile strain. It can be seen that, for −1% compressive strain the absolute value of the Seebeck coefficient increases by about 12%, while for tensile strain a drop of about 24% is found. As shown in Fig. 5(b), relaxation time scaled electrical conductivity σ/τ is significantly enhanced in these heavily doping regions. The electrical conductivity under strain in the inset of Fig. 5(b) states the opposite tendency compared with the Seebeck coefficient under applied strain. It is well known that strain-induced effects in the Seebeck coefficient and electrical conductivity tend to compensate each other.[19–21] As a consequence, there is an enhancement of the power factor of n-doped monolayer WSe_2 under compressive strain (Fig. 5(c), inset), and this is due to the enhancement of the Seebeck coefficient compared to the unstrained case. At the strain of −6% compressive strain, the Seebeck coefficient and the electrical conductivity attain their maximum and minimum at this magnitude and type of strain for n-type doping. As a result, the thermoelectric power factor reaches its maximum at this strain type and magnitude. Under tensile strain, the larger enhancement of the electrical conductivity cannot compensate the reduction of Seebeck coefficient, resulting in a reduction of the power factor of n-doped monolayer WSe_2, as shown in Fig. 5(c). Actually, WSe_2 is an intrinsic n-type semiconductor.[8] Since the power factor of n-doped monolayer WSe_2 can be increased by compressive strain, it can offer useful guidance on design and optimization of intrinsic monolayer WSe_2.

In order to explore in detail the dependence of thermoelectric properties in p-type doped monolayer WSe_2 on strain, the Seebeck coefficient, electrical conductivity, and power factors of p-doped monolayer WSe_2 as a function of the number of holes per unit cell are shown in Fig. 6, and the transport properties of monolayer WSe_2 at each given value of biaxial strain with the carrier concentration $p = 1.6\times10^{19}$ cm^{-3} are summarized in the inset of Fig. 6. As we can see from the inset of Fig. 6(a), the Seebeck coefficient increases first and then decreases with increasing tensile strain with a peak appearing under 4% strain, while

the value of the Seebeck coefficient slightly increases with the increasing compressive strain. Comparing with the Seebeck coefficient under strain, the opposite tendency emerges for the electrical conductivity under applied strain, namely, the electrical conductivity descends at first and then increases under tensile strain, while the electrical conductivity descends under compressive strain, as shown in the inset of Fig. 6(b). Combining the Seebeck coefficient with electrical conductivity, the results for the power factor under strain are shown in Fig. 6(c). For compressive strain, there emerges a slight reduction of power factor of p-doped monolayer WSe_2, and this is because there is only little enhancement of the Seebeck coefficient compared to the unstrained case. Under tensile strain, the enhancement of Seebeck coefficient makes it possible to compensate the reduction of electrical conductivity, resulting in an enhancement of power factor of p-doped monolayer WSe_2 when the strains are below 3%. Meanwhile, we note from the inset of Fig. 6(c) that the decrease of power

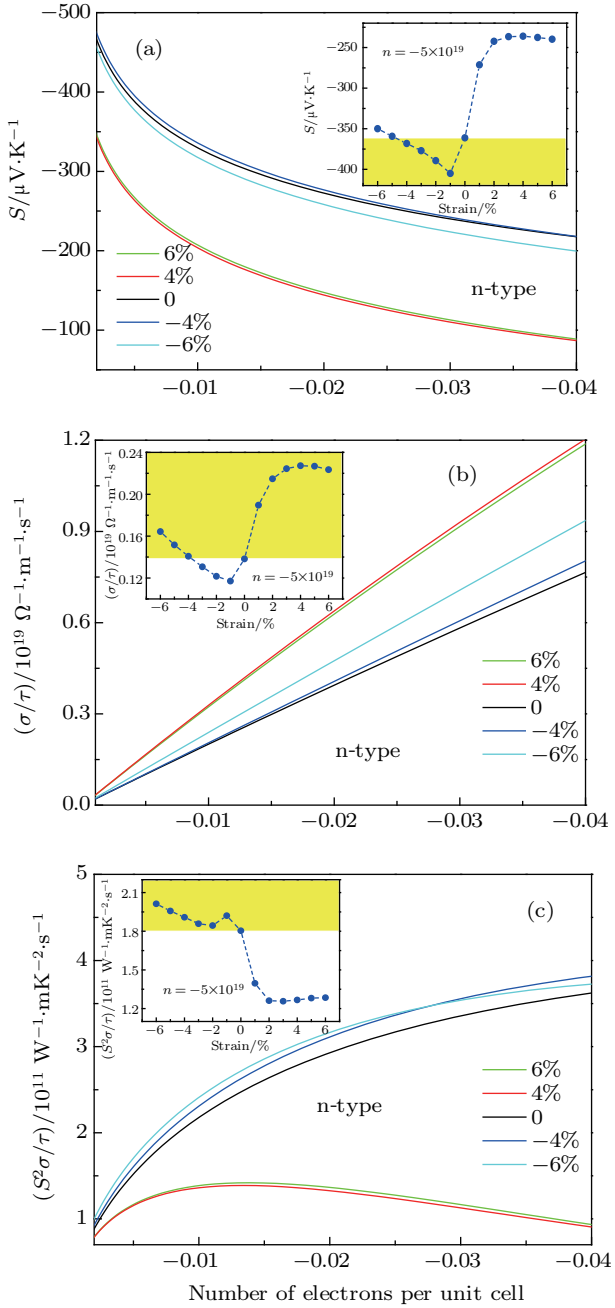


Fig. 5. (color online) Thermoelectric transport properties of n-doped monolayer WSe_2 as a function of electrons per unit cell at typical values of strain. (a) Seebeck coefficient. (b) The relaxation time scaled electrical conductivity. (c) Relaxation time scaled thermoelectric power factor. The insets are the thermoelectric transport properties of carrier n-doped monolayer WSe_2 at each given value of strain at 900 K with the electron concentration $n = -5 \times 10^{19}$ cm^{-3}. The range in which the thermoelectric transport properties are superior to the unstrained case is denoted with yellow.

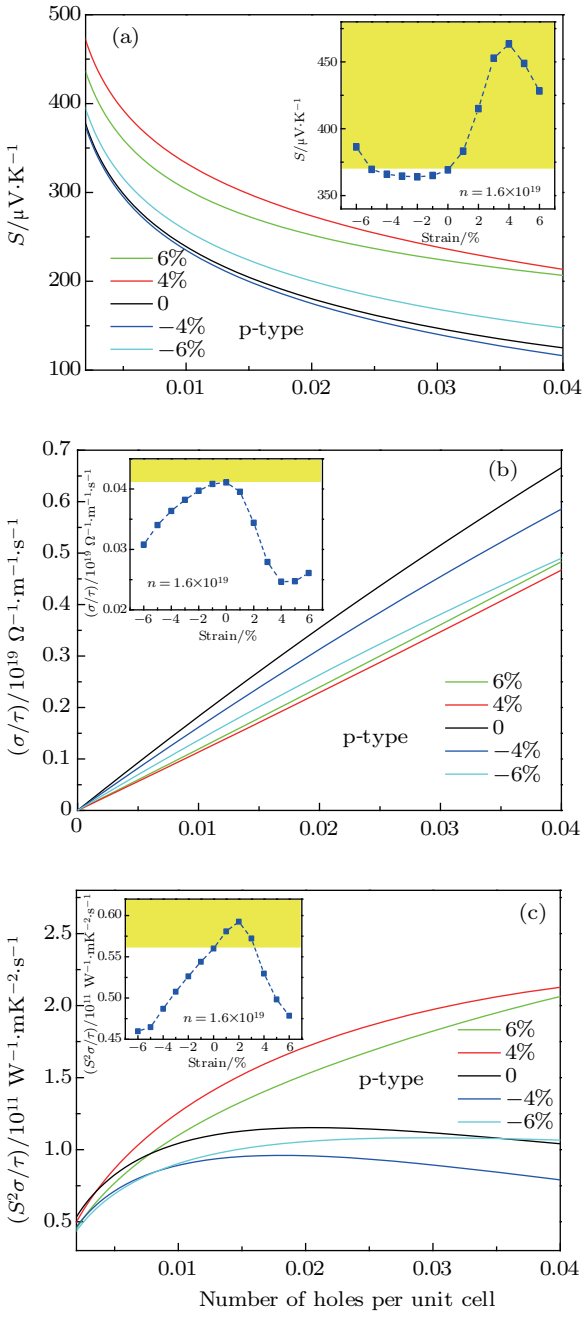


Fig. 6. (color online) Thermoelectric transport properties of p-doped monolayer WSe_2 as a function of electrons per unit cell at typical values of strain. (a) Seebeck coefficient. (b) The relaxation time scaled electrical conductivity. (c) Relaxation time scaled thermoelectric power factor. The insets are the thermoelectric transport properties of p-doped monolayer WSe_2 at each given value of strain at 900 K with the carrier concentration $p = 1.6 \times 10^{19}$ cm^{-3}. The range in which the thermoelectric transport properties are superior to the unstrained case is denoted with yellow.

factor of p-doped monolayer WSe_2 can be observed when the strain reaches 4%, suggesting that the over-strained band structure is not good for enhancement of thermoelectric performance.

In general, 2D transition metal dichalcogenides are n-type semiconductors.[8] The p-type doping of the 2D material can be achieved by chemical doping such as adsorption of small molecules.[42,43] As shown in Figs. 5(c) and 6(c), it is found that unstrained WSe_2 monolayer exhibits a higher value of power factor in n-type doping than in p-type doping. It can be seen that the relaxation time scaled power factor $S^2\sigma/\tau$ is 1.80×10^{11} $W\cdot K^{-2}\cdot m^{-1}\cdot s^{-1}$ in n-doped WSe_2 monolayer, while it is 0.56×10^{11} $W\cdot K^{-2}\cdot m^{-1}\cdot s^{-1}$ in p-type doping. Meanwhile, the maximum value attained by the Seebeck coefficient and the thermoelectric power factor for p-type doping at 2% and 4% tensile strain respectively is lower than the ones reached at 1% compressive strain for n-type doping. From such a comparative analysis, we can conclude that compressive strain applied to n-doped WSe_2 monolayer is found to be more effective than tensile strain applied on to p-doped WSe_2. In addition, both n-type doping under compressive strain and p-type doping under tensile strain, the enhancement of the power factor of monolayer WSe_2 can be achieved, suggesting that the applied strain is an efficient method for improving the thermoelectric performance of the monolayer WSe_2.

4. Conclusions

In summary, the influence of biaxial strain on the electronic structure and thermoelectric properties of monolayer WSe_2 have been investigated based on first-principles calculations. It is observed that the energy band gap of monolayer WSe_2 decreases with the application of biaxial strain, meanwhile, the dispersion of bands near Fermi level of monolayer WSe_2 are modified by biaxial strain. It is found that the shift of W d orbital near Fermi level from the projected DOS is caused by the change of W–Se bond length under strain, and it will shrink the band gap and change the shape of the band structure near the Fermi level. The transport properties of n- and p-doped monolayer WSe_2 under strain have been estimated based on semi-classical Boltzmann transport theory. Results suggest that compressive strain applied to n-doped WSe_2 monolayer is found to be more effective than tensile strain applied onto p-doped WSe_2. Meanwhile, it is found that both n-type doping under compressive strain and p-type doping under tensile strain can lead to enhancement of power factor in monolayer WSe_2. This research shows that the applied strain is an efficient route for improving the thermoelectric performance of monolayer WSe_2 and other 2D transition metal dichalcogenides materials.

References

[1] Chhowalla M, Shin H S, Eda G, Li L J, Loh K P and Zhang H 2013 *Nat. Chem.* **5** 263
[2] Liang W Y and Cundy S L 1969 *Philos. Mag.* **19** 1031
[3] Coehoorn R, Haas C, Dijkstra J, Flipse C J F, de Groot R A and Wold A 1987 *Phys. Rev. B* **35** 6195
[4] Benameur M M, Radisavljevic B, Heron J S, Sahoo S, Berger H and Kis A 2011 *Nanotechnology* **22** 125706
[5] Radisavljevic B, Radenovic A, Brivio J, Giacometti V and Kis A 2011 *Nat. Nano.* **6** 147
[6] Li H, Yin Z, He Q, Huang X, Lu G, Fam D W H, Tok A Y, Zhang Q and Zhang H 2012 *Small* **8** 63
[7] Johari P and Shenoy V B 2012 *ACS Nano* **6** 5449
[8] Bhattacharyya S, Pandey T and Singh A K 2014 *Nanotechnology* **25** 465701
[9] Amin B, Kaloni T P and Schwingenschlögl U 2014 *RSC Adv.* **4** 34561
[10] Guo S D 2016 *Comput. Mater. Sci.* **123** 8
[11] Kumar S and Schwingenschlögl U 2015 *Chem. Mater.* **27** 1278
[12] Huang W, Da H and Liang G 2013 *J. Appl. Phys.* **113** 104304
[13] Wickramaratne D, Zahid F and Lake R K 2014 *J. Chem. Phys.* **140** 124710
[14] Huang W, Luo X, Gan C K, S Y Quek and Liang G 2014 *Phys. Chem. Chem. Phys.* **16** 10866
[15] Hicks L D and Dresselhaus M S 1993 *Phys. Rev. B* **47** 12727
[16] Hicks L D and Dresselhaus M S 1993 *Phys. Rev. B* **47** 16631
[17] Zhou W X and Chen K Q 2015 *Sci. Rep.* **5** 15070
[18] Hinsche N F, Yavorsky B Y, Mertig I and Zahn P 2011 *Phys. Rev. B* **84** 165412
[19] Zou D, Nie G, Li Y, Xu Y, Zheng H and Li J 2015 *RSC Adv.* **5** 24908
[20] Zou D, Liu Y, Xie S, Lin J and Li J 2013 *Chem. Phys. Lett.* **586** 159
[21] Pardo V, Botana A S and Baldomir D 2013 *Phys. Rev. B* **87** 125148
[22] Zhang G and Zhang Y W 2015 *Mech. Mater.* **91** 382
[23] Dimple, Nityasagar J and Abir De S 2017 *J. Phys.: Condens. Matter* **29** 225501
[24] Chen K X, Wang X M, Mo D C and Lyu S S 2015 *J. Phys. Chem. C* **119** 26706
[25] Lv H, Lu W, Shao D, Lu H and Sun Y 2016 *J. Mater. Chem. C* **4** 4538
[26] Guo S D and Wang Y 2017 *Semicond. Sci. Tech.* **32** 055004
[27] Kresse G and Furthmüller J 1996 *Phys. Rev. B* **54** 11169
[28] Perdew J P, Burke K and Ernzerhof M 1996 *Phys. Rev. Lett.* **77** 3865
[29] Blöchl P E 1994 *Phys. Rev. B* **50** 17953
[30] Guo S D 2016 *J. Mater. Chem. C* **4** 9366
[31] Guo S D and Wang J L 2016 *Semicond. Sci. Tech.* **31** 095011
[32] Scheidemantel T J, Ambrosch-Draxl C, Thonhauser T, Badding J V and Sofo J O 2003 *Phys. Rev. B* **68** 125210
[33] Madsen G K H and Singh D J 2006 *Comput. Phys. Commun.* **175** 67
[34] Ong K P, Singh D J and Wu P 2011 *Phys. Rev. B* **83** 115110
[35] Guo H H, Yang T, Tao P and Zhang Z D 2013 *Chin. Phys. B* **22** 017201
[36] Kaur K and Kumar R 2016 *Chin. Phys. B* **25** 056401
[37] Kaur K and Kumar R 2016 *Chin. Phys. B* **25** 026402
[38] Peng H, Wang C L, Li J C, Zhang R Z, Wang H C and Sun Y 2011 *Chin. Phys. B* **20** 046103
[39] Schutte W J, De Boer J L and Jellinek F 1987 *J. Solid State Chem.* **70** 207
[40] Singh D J and Mazin I I 1997 *Phys. Rev. B* **56** R1650
[41] Lee M S, Poudeu F P and Mahanti S D 2011 *Phys. Rev. B* **83** 085204
[42] Mouri S, Miyauchi Y and Matsuda K 2013 *Nano Lett.* **13** 5944
[43] Zhao P, Kiriya D, Azcatl A, Zhang C, Tosun M, Liu Y S, Hettick M, Kang J S, McDonnell S, KC S, Guo J, Cho K, Wallace R M and Javey A 2014 *ACS Nano* **8** 10808